Accepted for publication in the Astrophysical Journal

Discovery of Twin Relativistic Jets in the Nearby E/S0 Galaxy NGC 3894

G. B. Taylor & J. M. Wrobel
National Radio Astronomy Observatory,
P.O. Box O, Socorro, New Mexico 87801
(e-mail: gtaylor@nrao.edu, jwrobel@nrao.edu)

and

R. C. Vermeulen
Netherlands Foundation for Research in Astronomy,
P.O. Box 2, NL-7990 AA Dwingeloo, The Netherlands
(e-mail: rcv@nfra.nl)

ABSTRACT

VLBI techniques were used to monitor the milliarcsecond-scale continuum structure of the E/S0 galaxy NGC 3894. The resulting VLBI images span 15 years, and provide morphological and spectral evidence for twin, parsec-scale jets emerging from a synchrotron-self-absorbed core. Analysis of the twin-jet kinematics requires that the jets be both mildly relativistic ($v \sim 0.3c$) and oriented well away from the line of sight ($\theta \sim 50°$). Slow jets could be deflected or disrupted, so evidence for such processes is examined. A large viewing angle could influence the galaxy's nuclear properties at other wavebands, and those properties are explored.

Subject headings: galaxies: elliptical and lenticular, cD - galaxies: jets - galaxies: nuclei - galaxies: individual (NGC 3894, UGC 06779, 1146+596) - radio continuum: galaxies

1. Introduction

Starlight dominates the optical continuum emission from the bright and large galaxy NGC 3894 (UGC 06779), which has been variously classified as an elliptical or a lenticular (E4, de Vaucouleurs et al. 1991; S0, Nilson 1973). In contrast, the galaxy's radio and far-infrared continuum led Condon & Broderick (1988) to conclude that the primary radio energy source must be a "monster", most probably a supermassive black hole. At arcsecond resolution, the radio emission is dominated by a compact component with a flat spectrum (Condon & Dressel 1978; Wrobel & Heeschen 1984). Neutral hydrogen is detected in absorption against this component (van Gorkom et al. 1989). Both a dust lane and ionized gas are distributed along the galaxy's major axis, with the ionized gas exhibiting LINER properties and pronounced noncircular motions (Kim 1989). For $q_0 = 0.5$ and $H_0 = 100\,h$ km s^{-1} Mpc^{-1}, the optical absorption redshift $z = 0.01085$ (van Gorkom et al. 1989) implies a luminosity distance of $32.6\,h^{-1}$ Mpc and scales of 1 arcsec = $155\,h^{-1}$ pc.

At milliarcsecond resolution, VLBI imaging of NGC 3894 at 5.0 GHz revealed 3 components defining an elongated structure with a projected extent of $0.9\,h^{-1}$ pc (Wrobel, Jones & Shaffer 1985). The component strengths were consistent with the asymmetric "core-jet" morphology typical of flat-spectrum extragalactic radio sources, and usually interpreted in terms of Doppler boosting in opposed relativistic jets oriented close to the line of site (e.g., Kellermann & Pauliny-Toth 1981). However, for NGC 3894 the "core-jet" interpretation was hampered by severe component blending and the absence of spectral data needed to separate a synchrotron-self-absorbed "core" from steeper-spectrum jet material. Indeed, the galaxy's low radio power of $8.2 \times 10^{22}\,h^{-2}$ W Hz^{-1} at 5.0 GHz (Wrobel & Heeschen 1984) might be ascribed to opposed jets with a substantial viewing angle; if so, then both jets could be detected, leading to a symmetric, not asymmetric, morphology. Further VLBI imaging of NGC 3894 was needed to resolve this dilemma. VLBI monitoring at 5.0 GHz could track component motion away from any "core", removing blending problems; while VLBI spectral index data can help isolate any "core". This paper reports such observations of NGC 3894, and provides morphological and spectral evidence for twin, parsec-scale jets emerging from a synchrotron-self-absorbed core. The twin-jet kinematics requires that the jets are mildly relativistic ($v \sim 0.3c$ for $h = 0.5$) and tilted well away from the line of sight ($\theta \sim 50°$).

2. Observations

2.1. VLBI

The first VLBI imaging observations of NGC 3894 were made at epoch 1981 (Wrobel, Jones & Shaffer 1985), and will be referred to as the first epoch for a series of observations at 5.0 GHz. A second, more sensitive observation at 5.0 GHz was obtained in 1989 using the NRAO VLA in phased-array mode, Bonn, Owens Valley 40-m, NRAO 140-ft, Haystack, Fort Davis, Bologna, Jodrell Bank Mk2, Westerbork in phased-array mode, and the NRAO VLBA antenna at Pie Town, New Mexico. Details of this and other VLBI epochs are summarized in Table 1. In 1992 NGC 3894 was again observed at 5.0 GHz using a global array as part of the Second Caltech-Jodrell Bank VLBI survey (Taylor et al. 1994). Fourth and fifth epochs at 5.0 GHz were obtained in 1994 and 1996, respectively, as part of a proper motion study (Vermeulen et al. 1997). Finally, NGC 3894 was also observed in 1995 at 8.4 and 1.4 GHz with the VLBA recording 32 MHz total bandwidth with 2-bit sampling. All VLBI data were acquired in left circular polarization. Napier et al. (1994) provide a full description of the VLBA.

2.2. VLA

During the second VLBI epoch, VLA data were acquired on NGC 3894 in dual circular polarizations with a bandwidth of 50 MHz centered at 4985 MHz, with the VLA being "auto-phased" in the manner described by Wrobel (1983). The VLA was also used briefly in its standard phase-referencing mode on 1989 April 13 to acquire snapshots of NGC 3894 in dual circular polarizations with a bandwidth of 50 MHz, centered on frequencies of 4835, 4885, 8415, 8465, 14915, and 14965 MHz. The source 3C 286 was observed as a primary flux density calibrator. The VLA was in its B configuration with 25-27 antennas available during 1989 April. Thompson et al. (1980) describe the VLA.

3. Analysis

3.1. VLBI

The first epoch at 5.0 GHz was imaged and CLEANed using Difmap (Shepherd, Pearson & Taylor 1994, 1995). Data from all other epochs were calibrated, fringe-fitted, imaged, and CLEANed using NRAO AIPS software and Difmap, as described by Taylor et al. (1994). A montage of all five VLBI images at 5.0 GHz appears in Fig. 1. Difmap was used to model-fit Gaussian components to the self-calibrated visibility data from each 5.0 GHz epoch. The shapes of 4 components were fixed after fitting to the most sensitive (1989) epoch; these shapes are given in Table 2 and the 4 components are labeled in Fig. 1 at epoch 1989. At subsequent 5.0 GHz epochs, only 3 components were fitted, and each Gaussian component was allowed only to move and to vary in flux density in order to fit the independently self-calibrated visibility data from those epochs. This source is not well described by simple Gaussian components, so the fits obtained were relatively poor and must be interpreted with some caution. The positions of all components are quoted with respect to the VLBI core component, discussed in Section 4.1.

3.2. VLA

The phased VLA data at 5.0 GHz on NGC 3894 were calibrated in AIPS as described by Wrobel (1983), with the added improvement that non-closing correlator errors were determined from the strong, compact source 4C 39.25 and removed from the NGC 3894 data. Fig. 2 shows the resulting CLEANed image of NGC 3894 made with uniform weighting of the visibility data.

The formal dynamic range (peak/rms) of this deep VLA image is about 22,000. For comparison purposes, Fig. 2 also shows a CLEANed VLA image at 1.5 GHz (Condon, Machalski & Wrobel 1997). That VLA snapshot image has a slightly poorer resolution, and a much lower sensitivity, than the phased VLA image at 5.0 GHz. Nonetheless, the 1.5 GHz image is a useful independent check on the reality of the very weak extended structures evident in the phased VLA image at 5.0 GHz.

The VLA data acquired 1989 April 13 were calibrated, imaged and CLEANed as described by Wrobel & Heeschen (1991). The following flux densities were derived for NGC 3894: 568 ± 17, 568 ± 17, 518 ± 16, 518 ± 16, 447 ± 22, and 449 ± 22 mJy at frequencies of 4835, 4885, 8415, 8465, 14915, and 14965 MHz, respectively. Although the VLA correlator provided parallel and crossed-hand data on both April 13 and 14, only the parallel hands were analyzed. Upper limits to the linearly polarized emission from NGC 3894 are given by Wrobel & Heeschen (1984) and Taylor et al. (1996).

The new VLA spectral results for epoch 1989 are plotted in Fig. 3. Also appearing in Fig. 3 are earlier published spectral data (epoch 1980, Wrobel & Heeschen 1984; Wrobel, Jones & Shaffer 1985), plus contemporaneous millimeter and submillimeter results (epoch 1989, Knapp & Patten 1991) and VLBA results from this work (epochs 1994 and 1995). Fig. 3 provides evidence for spectral variability. To better define the variability time scale, the flux density history of NGC 3894 in the 6 cm and 20 cm regions was assembled from the literature and plotted in Fig. 4. See that figure's caption for references and other details. Also indicated in the bottom of Fig. 4 are the VLBI epochs listed in Table 1, with the plotted symbols coding an observation at 5.0 GHz (6 cm) or 1.4 GHz (20 cm).

4. Discussion

4.1. Twin Jets on Parsec Scales

The VLBA image at 8.4-GHz (Fig. 2) is restored with the same 2-mas ($0.31\,h^{-1}$ pc) CLEAN beam as that used for the 5.0 GHz images in Fig. 1. The enhanced emission of the compact, central component at 8.4 GHz indicates an inverted spectrum. This component is labeled as "C" in Fig. 2, while Fig. 3 shows that its spectral index is $\alpha = 0.77 \pm 0.14$ ($S \propto \nu^{+\alpha}$). This contrasts with the strong, resolved NW jet that Fig. 3 shows has a steeper spectrum with $\alpha = -0.25 \pm 0.14$. Thus, based on its enhanced strength, compactness, and inverted spectrum, the central component is identified with the center of activity in the milliarcsecond structure. While we cannot rule out the possibility that this component is free-free absorbed at low frequencies, given its strength and compactness, synchrotron self-absorption seems the more natural explanation. Identification of this central component as the "core" gives the source a symmetric appearance on milliarcsecond scales: twin jets straddle the core. This is contrary to the asymmetric, core-jet interpretation offered by Wrobel, Jones & Shaffer (1985) based only on the topmost image in Fig. 1. From Fig. 1

alone, it may seem inappropriate to apply the term "jet" to the resolved NW and SE components. However, the terminology is justified once the images in Fig. 1 are examined in conjunction with the lower-resolution VLBA image at 1.4 GHz in Fig. 2.

4.2. Parsec-Scale Kinematics

From comparison of the first and subsequent epochs in Fig. 1, it is clear that the source is growing to the NW and SE. Component growth is also implied by the shift in the maximum "total" source flux density to lower frequencies (Fig. 4). The simplest explanation is that material in the twin jets is moving away from the center of activity. Fig. 5 shows the peak offsets from Table 2 of the NW and SE jets, relative to the core. Based on Fig. 5, the NW jet exhibits a steady proper motion of 0.19±0.01 mas yr^{-1} along position angle $-46°$. The case for motion to the SE is unclear from Fig. 5, but is evident from visual inspection of Fig. 1. To better define the overall growth of the source, the NW and SE edges of the source were measured at the 8 mJy beam^{-1} level (see the crosses in Fig. 1). This yields a proper motion to the NW of 0.26±0.05 mas yr^{-1} and to the SE of 0.19±0.05 mas yr^{-1}.

In the simple beaming model for a twin-jet system, both the arm length ratio D and the flux density ratio R depend on the intrinsic jet speed $\beta = v/c$ and on the angle of the twin jets to the line of sight θ (Taylor & Vermeulen 1997). Specifically, the arm length ratio is

$$D = \frac{\mu_{\rm a}}{\mu_{\rm r}} = \frac{d_{\rm a}}{d_{\rm r}} = \left(\frac{1+\beta\cos\theta}{1-\beta\cos\theta}\right) \tag{1}$$

where the apparent projected distances from the origin are $d_{\rm a}$ for the approaching side and $d_{\rm r}$ for the receding side, and the apparent proper motions are $\mu_{\rm a}$ for the approaching side and $\mu_{\rm r}$ for the receding side. The β in Equation (1) refers to a pattern speed. Similarly, the flux density ratio between the approaching side $S_{\rm a}$ and the receding side $S_{\rm r}$ is

$$R = \frac{S_{\rm a}}{S_{\rm r}} = \left(\frac{1+\beta\cos\theta}{1-\beta\cos\theta}\right)^{k-\alpha}, \tag{2}$$

where α is the spectral index, $k = 2$ for a continuous jet and $k = 3$ for discrete jet components (but see e.g. Lind & Blandford 1985). The β in Equation (2) refers to a fluid speed.

Equations (1) and (2) can be used to constrain the product $\beta\cos\theta$ for NGC 3894, on the assumptions that the center of activity is located at the core and that the NW and SE jet components were ejected simultaneously from this center of activity. Since the jet components are still rather close to the core, any analysis based on these inner knots may suffer from systematic errors due to blending of the features; indeed, this is almost certainly the case for the first epoch at 5.0 GHz. The jet positions in Table 2 consistently require that the NW jet is approaching and the SE jet is receding. At the latest available epoch the resulting arm length ratio from Equation (1) implies $\beta\cos\theta = 0.18 \pm 0.03$; this constraining region lies between the solid lines in Fig. 6. The flux density ratio from Equation (2) at the same epoch requires $\beta\cos\theta \sim 0.1$ for $k = 2$, in fairly close agreement given that the jet flux densities are not well modeled by simple Gaussians, and the fluid and pattern β's may differ.

Another constraint on the two parameters β and θ for NGC 3894 can be obtained from the overall separation velocity $v_{\rm sep} = |v_{\rm a}| + |v_{\rm r}|$, which, unlike $v_{\rm a}/v_{\rm r}$, is not subject to reference point uncertainties (Taylor & Vermeulen 1997):

$$v_{sep} = \mu_{sep}\, D_\theta\, (1+z) = \frac{2\beta c \sin\theta}{(1-\beta^2\cos^2\theta)}\,, \qquad (3)$$

where β refers to a pattern speed and, for NGC 3894, the redshift z is from van Gorkom et al. (1989) and the angular size distance $D_\theta = 31.9\,h^{-1}$ Mpc. Summing the NW and SE proper motions measured at the 8-mJy level, Equation (3) implies $v_{\rm sep} = 0.23 \pm 0.05\,h^{-1}c$ and leads, in turn, to the constraining region between the dotted lines in Fig. 6. The overlap region in Fig. 6 requires that the twin parsec-scale jets in NGC 3894 be both mildly relativistic ($v \sim 0.3c$ for $h = 0.5$) and oriented well away from the line of sight ($\theta \sim 50°$).

At epoch 1996, the summed arm lengths divided by the summed proper motions implies that the NW and SE jets emerged from the core about 21 years previously, in 1975. A small source size in 1975 should cause a strongly synchrotron-self-absorbed spectrum, consistent with the "total" flux densities near that epoch in Fig. 4.

4.3. Implications of the Jet Speed

Mildly relativistic ($v \sim 0.3c$ for $h = 0.5$) jets could be deflected or disrupted. This section examines the evidence for such processes.

The VLBA image at 1.4 GHz (Fig. 2) shows that the SE jet continues to ~ 20 mas ($3.1\,h^{-1}$ pc) in projection from the core and abruptly bends to point almost due south. A much fainter jet is evident to the NW extending nearly 100 mas ($16\,h^{-1}$ pc) in projection. These outer jets themselves must bend substantially to match the almost east-west extensions seen in the VLA images in Fig. 2 on a projected scale of ~ 3 arcsec ($460\,h^{-1}$ pc). Sensitive continuum observations on scales intermediate between those probed by the VLBA and VLA are required to trace these bends and understand their origin. In the interim, however, four points are worth mentioning, each of which suggests dynamical interaction between the jets and the interstellar medium in NGC 3894.

First, the position angle of the "final" radio elongation means that the radio source appears to emerge along the optical minor axis (110°, Condon et al. 1991 and Fig. 2). If NGC 3894 is an oblate rotator, then such minor axis ejection is energetically favored. Second, the rapid fading of the jets beyond ~ 3 arcsec ($460\,h^{-1}$ pc) might occur because ambient gas pressures along the minor axis are too low to confine the jets, or because the jets are substantially slowed because they entrain ambient gas. Third, Kim (1989) finds that, over the central few arcseconds, the major-axis kinematics of the optical line-emitting gas is very peculiar: it first increases very rapidly, then suddenly decreases, and finally reaches a roughly constant velocity. Such noncircular motions could arise because the radio jets exert nongravitational forces on the line-emitting gas. Fourth, the LINER spectrum of the the extended line-emitting gas (Kim 1989) could signal shock excitation, again suggesting dynamical interaction with the radio jets. Collectively, these four points hint at jet/gas interaction within the inner few arcseconds of NGC 3894, and provide strong motivation to quantify the properties of the nuclear interstellar medium.

4.4. Implications of the Viewing Angle

A large viewing angle reduces Doppler boosting effects, which could impact the galaxy's nuclear properties at other wavebands. Those properties are explored in this section.

Patnaik et al. (1992) used the VLA to measure the following position, accurate to 12 mas, for the dominant compact component in NGC 3894: $\alpha(J2000) = 11^h48^m50\overset{s}{.}3591$, $\delta(J2000) = 59°24'56\overset{''}{.}362$. Armed with this radio position, does one expect to find corresponding emission from NGC 3894 at other wavebands? This is very unlikely, based on the rapid downturn of the total radio spectrum evident in Fig. 3. Indeed, Heckman et al. (1983) find no nonstellar continuum from NGC 3894 at 3850Å. However, both those authors and Puschell (1981) report evidence for a nonstellar continuum source in the near-infrared. Puschell (1981) finds that the infrared source lies well above an extrapolation of the radio continuum at epoch 1980, so it must be unrelated to that continuum; rather, it could arise either from a thermally-reradiating dust cloud or a separate synchrotron source.

4.5. Comparisons to High Luminosity Compact Symmetric Objects

Aside from a radio luminosity 3 orders of magnitude lower, there is considerable similarity between the properties of NGC 3894 and the Compact Symmetric Objects (CSOs) studied by Readhead et al. (1996a), and Taylor, Readhead, & Pearson (1996). Also, the only source besides NGC 3894 to show bi-directional motion in its jets is the CSO 1946+708 (Taylor & Vermeulen 1997). The CSOs are defined as sources less than 1 kpc in size, having radio emission on both sides of the central engine that is thought to be relatively free of beaming effects (Wilkinson et al. 1994). CSOs comprise $\sim$5% of sources in complete flux-limited samples selected at high frequencies. Nearly all CSOs have two steep-spectrum hot spots and/or lobes and most have an inverted or flat-spectrum core (Taylor et al. 1996). Some other properties are low polarization, steep spectra at high frequencies, bright elliptical galaxy hosts, weak ($<$ 5%/yr) radio variability, and very low core luminosities. NGC 3894 differs from CSOs in having a larger fraction of its radio luminosity in the component we have identified as the core, and in having greater variability.

The favored interpretation for the CSOs is that they are young objects that evolve into compact steep spectrum doubles and then into FR II classical doubles (Readhead et al. 1996b). NGC 3894 could be a young object (age $\sim 10^4$ yrs), only if the jets remain relativistic out to the emission seen on the arcsecond scale, or if this emission has another origin, such as a previous phase of activity. If NGC 3894 evolves in luminosity in a similar fashion to the CSOs, then unlike CSOs it must evolve into a FR I radio galaxy.

5. Conclusions

The parsec-scale structure of the nearby E/S0 galaxy NGC 3894 was monitored from 1981 to 1996 with VLBI techniques. Morphological and spectral evidence imply that twin, parsec-scale jets emerge from a synchrotron-self-absorbed core. The kinematics of the twin jets demands that they are both mildly relativistic ($v \sim 0.3c$ for $h = 0.5$) and tilted well away from the line of sight ($\theta \sim 50°$). There are hints that these slow jets are interacting dynamically with the nuclear interstellar medium. The galaxy shows no evidence for infrared or optical continuum related to the parsec-scale radio emission, consistent with the large viewing angle inferred for that radio emission.

We thank the observatory and correlator staffs for their assistance. This work was supported in part by the NSF under grants AST-8611247, AST-9117100 and AST-9420018. The National Radio Astronomy Observatory is operated by Associated Universities, Inc., under cooperative agreement with the National Science Foundation.

Table 1. VLBI Observational Parameters for NGC 3894

VLBI Epoch	Frequency (GHz)	Bandwidth (MHz)	Number of Antennas	Scan Length (min)	Total Time (hours)
1981 Dec 7	5.0	2	6	30	9.92
1989 Apr 14	5.0	2	10	30	15.35
1992 Sep 25	5.0	2	15	20	0.90
1994 Sep 15	5.0	2	10	20	0.98
1995 Mar 22	8.4	16	10	6	0.49
	1.4	16	10	6	0.99
1996 Aug 24	5.0	8	10	5	0.70

Table 2. VLBI Gaussian Models for NGC 3894 at 5 GHz

Component	Epoch (yr)	S (mJy)	r (mas)	θ (°)	a (mas)	b/a	Φ (°)
NW jet	1989.3	261	4.19	−48.4	3.23	0.51	−48.0
	1992.2	306	4.99	−42.8	3.23	0.51	−48.0
	1994.7	234	5.09	−46.8	3.23	0.51	−48.0
	1996.6	187	5.70	−46.3	3.23	0.51	−48.0
Core	1989.3	110	0.00	0.0	0.81	0.58	−64.4
	1992.2	87	0.00	0.0	0.81	0.58	−64.4
	1994.7	79	0.00	0.0	0.81	0.58	−64.4
	1996.6	67	0.00	0.0	0.81	0.58	−64.4
SE jet	1989.3	123	4.12	138.7	3.26	0.38	−31.1
	1992.2	100	3.85	136.9	3.26	0.38	−31.1
	1994.7	114	3.73	140.9	3.26	0.38	−31.1
	1996.6	121	3.95	141.5	3.26	0.38	−31.1
SE lobe	1989.3	31	14.32	163.1	14.78	0.51	8.4

Note. — Parameters of each Gaussian component of the model brightness distribution: S, flux density; r, θ, polar coordinates of the center of the component relative to an arbitrary origin, with polar angle measured from north through east; a, b, major and minor axes of the FWHM contour; Φ, position angle of the major axis measured from north through east.

REFERENCES

Condon, J. J., & Dressel, L. L. 1978, ApJ, 221, 456

Condon, J. J., & Broderick, J. J. 1988, AJ, 96, 30

Condon, J. J., Frayer, D. T., & Broderick, J. J. 1991, AJ, 101, 362

Condon, J. J., Machalski, J., & Wrobel, J. M. 1997, in preparation

de Vaucouleurs, G., de Vaucouleurs, A., Corwin, Jr, H. G., Buta, R. J., Paturel, G., & Fouque, P. 1991, The Third Reference Catalog of Bright Galaxies (New York: Springer-Verlag)

Fabbiano, G., Gioia, I., & Trinchieri, G. 1989, ApJ, 347, 127

Heckman, T. M., Lebofsky, M. J., Rieke, G. H., & van Breugel, W. 1981, ApJ, 272, 400

Kapahi, V. K. 1979, A&A, 74, L11

Kellermann, K. I., & Pauliny-Toth, I. I. K. 1981, ARA&A, 19, 373

Kim, D.-W. 1989, ApJ, 346, 653

Knapp, G. R., & Patten, B. M. 1991, AJ, 101, 1609

Lind, K. R., & Blandford, R. D. 1985, ApJ, 295, 358

Nilson, P. 1973, Uppsala General Catalog of Galaxies (Uppsala: Uppsala Astronomical Observatory)

Napier, P. J., Bagri, D. S., Clark, B. G., Rogers, A. E. E., Romney, J. D., Thompson, A. R., & Walker, R. C. 1994, Proc. IEEE, 82, 658

Patnaik, A. R., Browne, I. W. A., Wilkinson, P. N., & Wrobel, J. M. 1992, MNRAS, 254, 655

Puschell, J. J. 1981, ApJ, 247, 48

Readhead, A. C. S., Taylor, G. B., Xu, W., Pearson, T. J., Wilkinson, P. N., & Polatidis, A. G. 1996a, ApJ, 460, 612

Readhead, A. C. S., Taylor, G. B., Pearson, T. J., & Wilkinson, P. N. 1996b, ApJ, 460, 634

Shepherd, M. C., Pearson, T. J., & Taylor, G. B. 1994, BAAS, 26, 987

Shepherd, M. C., Pearson, T. J., & Taylor, G. B. 1995, BAAS, 27, 903

Thompson, A. R., Clark, B. G., Wade, C. M., Napier, P. J., 1980, ApJS, 44, 151

Taylor, G. B., Vermeulen, R. C., Pearson, T. J., Readhead, A. C. S., Henstock, D. R., Browne, I. W. A., & Wilkinson, P. N. 1994, ApJS, 95, 345

Taylor, G. B., Vermeulen, R. C., Readhead, A. C. S., Pearson, T. J., Henstock, D. R., & Wilkinson, P. N. 1996, ApJS, 107, 37

Taylor, G. B., Readhead, A. C. S., & Pearson, T. J. 1996, ApJ, 463, 95

Taylor, G. B., & Vermeulen, R. C. 1997, ApJ, 485, L9 van Gorkom, J. H., Knapp, G. R., Ekers, R. D., Ekers, D. D., Laing, R. A., & Polk, K. S. 1989, AJ, 97, 708

Vermeulen, R. C. et al. 1997, in preparation

Wilkinson, P. N., Polatidis, A. G., Readhead, A. C. S., Xu, W. , & Pearson, T. J. 1994, ApJ, 432, L87

Wrobel, J. M. 1983, AJ, 88, 1757

Wrobel, J. M. & Heeschen, D. S. 1984, ApJ, 287, 41

Wrobel, J. M. & Heeschen, D. S. 1991, AJ, 101, 148

Wrobel, J. M., Jones, D. L., & Shaffer, D. B. 1985, ApJ, 289, 598

Fig. 1.— Time montage of CLEANed VLBI images of NGC 3894 at 5.0 GHz from 1981 to 1996. The synthesized restoring beam for each image has a FWHM of 2 mas ($0.31\,h^{-1}$ pc) and is drawn in the lower left-hand corner of the montage. Contours are drawn logarithmically at factor of 2 intervals, with the first positive contour at 2, 0.5, 2, 2, and 1 mJy beam^{-1} for epochs 1981–1996, respectively. The crosses mark the NW and SE edges of the source at the 8 mJy beam^{-1} level. Component labels are as for Table 2.

Fig. 2.— Angle montage of CLEANed images of NGC 3894 from arcsecond to mas scales. The restoring beam is 1.8, 1, 0.01×0.005 in position angle 10°, and 0.002 arcsec going from top to bottom. Contours are drawn at 660, 57, 350, and 650 microJy beam^{-1} $\times$ (-2, -1, 1, 2, 3, 4, 5.6, 6, 8, etc. increasing by root 2) in the images from top to bottom, respectively. The component labeled "C" in the VLBA image at 8.4 GHz is identified as the core.

Fig. 3.— Continuum spectrum of NGC 3894. Symbols encode spectra from VLA and single dish data near 1980 (filled squares) and 1989 (crosses and upper limits), and show VLBA flux densities for the NW jet (open triangles) and core component (open circles) at close epochs 1994 and 1995. An amplitude error of 5% was assumed for the VLBA data. New VLA data are from Section 3.2. See text for references to published work.

Fig. 4.— Flux density history of NGC 3894 over the past 20 years in the 20 cm and 6 cm regions. The angular resolutions range from 24 to 0.5 arcsec. Integration over a 10 by 10 arcsec region was done for 20 cm data with resolutions similar to that of the VLA images in Fig. 2. New VLA data are from Section 3.2. Published data have the following epoch, frequency and reference: 1977, 1415 and 4995 MHz, Kapahi 1979; 1980.940, 1465 and 4885 MHz, Wrobel & Heeschen 1984; 1981.934, 4985 MHz, Wrobel 1983; 1985.592, 1465 MHz, Wrobel, unpublished; 1986.915, 1490 MHz, Condon & Broderick 1988; 1987.792, 4860 MHz, Fabbiano et al. 1989; 1988.997, 1490 MHz, Condon, Machalski & Wrobel 1997; 1994.587, 4535 MHz, Taylor et al. 1996; 1995.523, 1415 MHz, Taylor et al. 1996. If a published reference quotes an observation date, then the assigned epoch error is ± 1 day. If only the dates spanned by the observing session are quoted, then the epoch error reflects those dates. No epoch information was provided by Kapahi (1979); at that author's suggestion, the epoch was assumed to be the same as that of similar work published close in time and a generous error of ± 2 years was assigned.

Fig. 5.— Trajectories from Table 2 for the NW and SW jets relative to the core in NGC 3894. Epochs 1989, 1992, 1994, and 1996 are plotted with symbols 2, 3, 4, and 5, respectively.

Fig. 6.— Pattern speed $\beta = v/c$ plotted against the line-of-sight viewing angle θ for NGC 3894. The solid lines follow from the arm length ratio deduced from Equation (1), while the dotted lines are the result of the overall separation growth based on Equation (3) for $h = 0.5$ and $h = 1$. The constraints common to the overlap region mean that the twin parsec-scale jets in NGC 3894 are both mildly relativistic ($v \sim 0.3c$ for $h = 0.5$) and tipped well away from the line of sight ($\theta \sim 50°$).

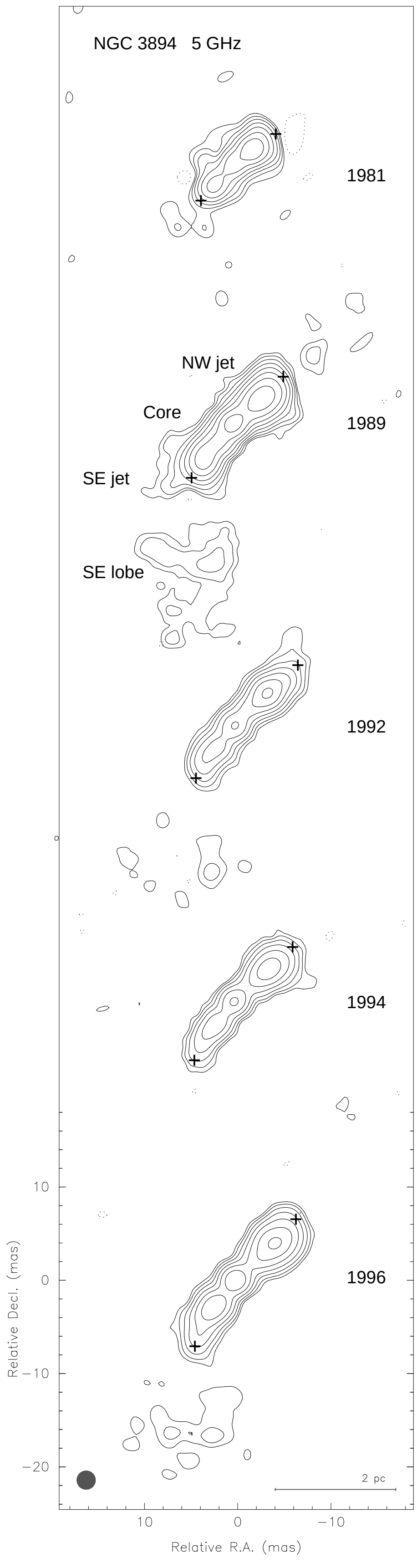

NGC 3894 5 GHz
1981
NW jet
Core
SE jet
1989
SE lobe
1992
1994
1996
2 pc
Relative Decl. (mas)
10
0
−10
−20
Relative R.A. (mas)
10
0
−10

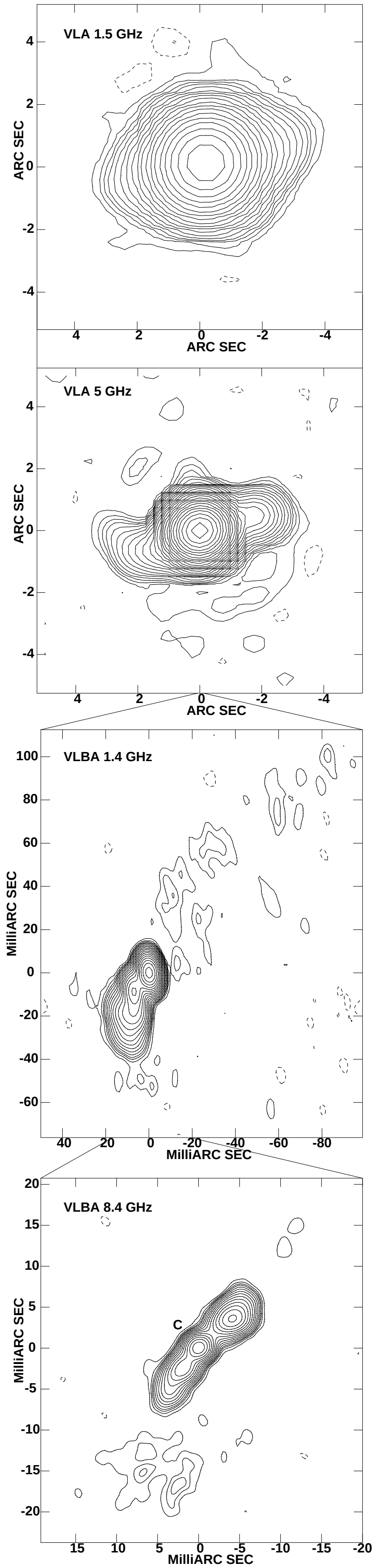
VLA 1.5 GHz
ARC SEC
ARC SEC
VLA 5 GHz
ARC SEC
ARC SEC
VLBA 1.4 GHz
MilliARC SEC
MilliARC SEC
VLBA 8.4 GHz
C
MilliARC SEC
MilliARC SEC

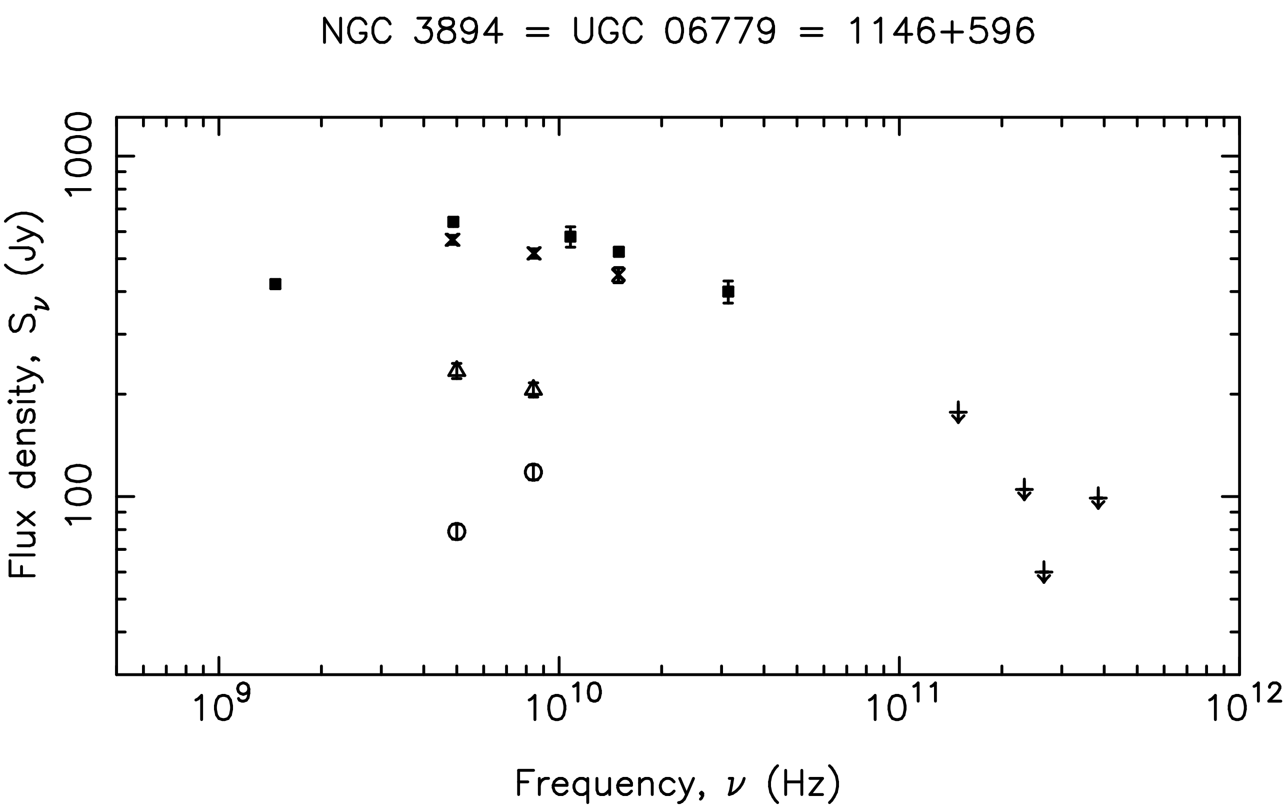
NGC 3894 = UGC 06779 = 1146+596
Flux density, S_ν (Jy)
Frequency, ν (Hz)
1000
100
10^9
10^{10}
10^{11}
10^{12}

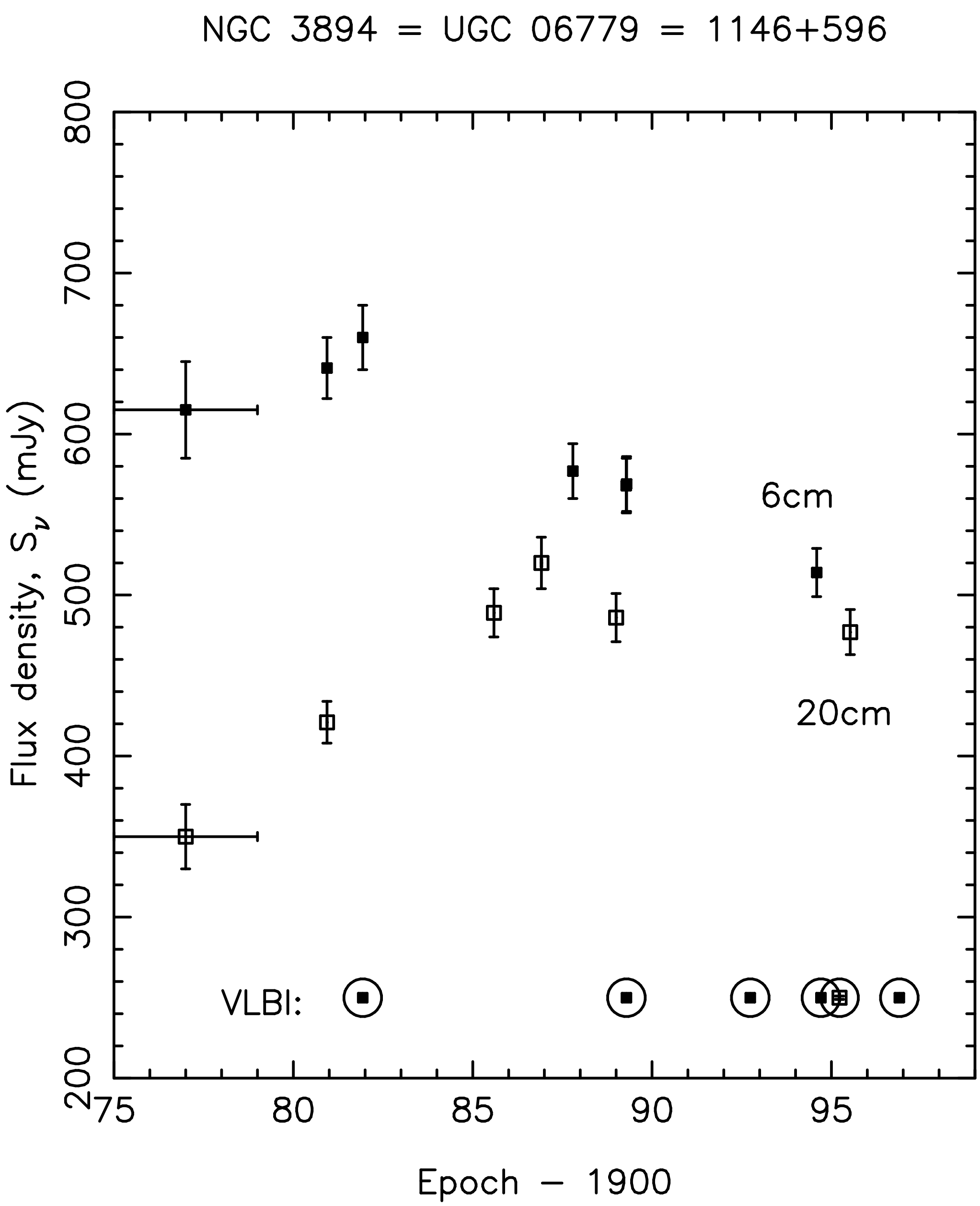
NGC 3894 = UGC 06779 = 1146+596
Flux density, S_ν (mJy)
800
700
600
500
400
300
200
6cm
20cm
VLBI:
75
80
85
90
95
Epoch − 1900

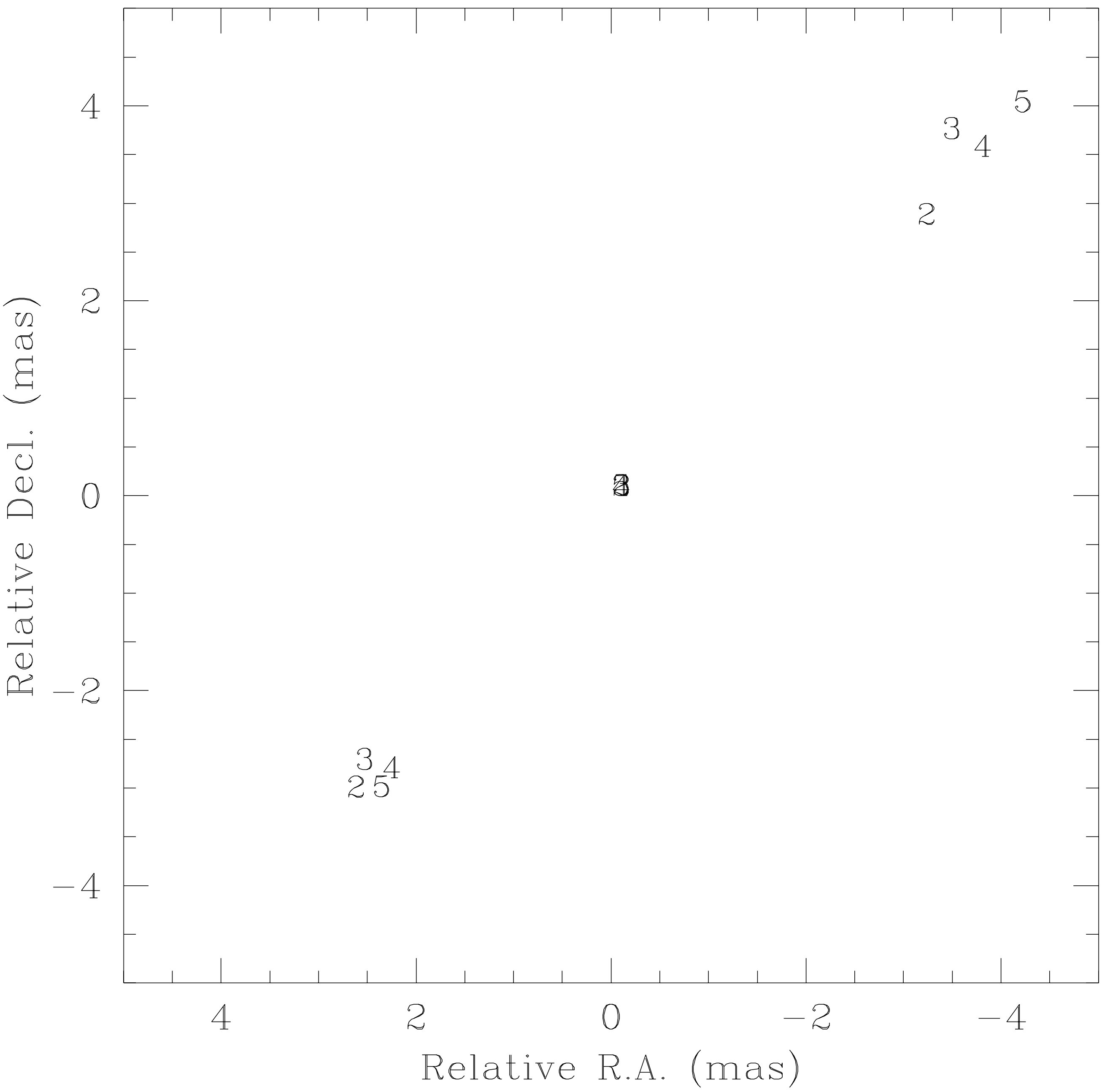
Relative Decl. (mas)
Relative R.A. (mas)
4
2
0
−2
−4
3
4
5
2
3
4
2
5

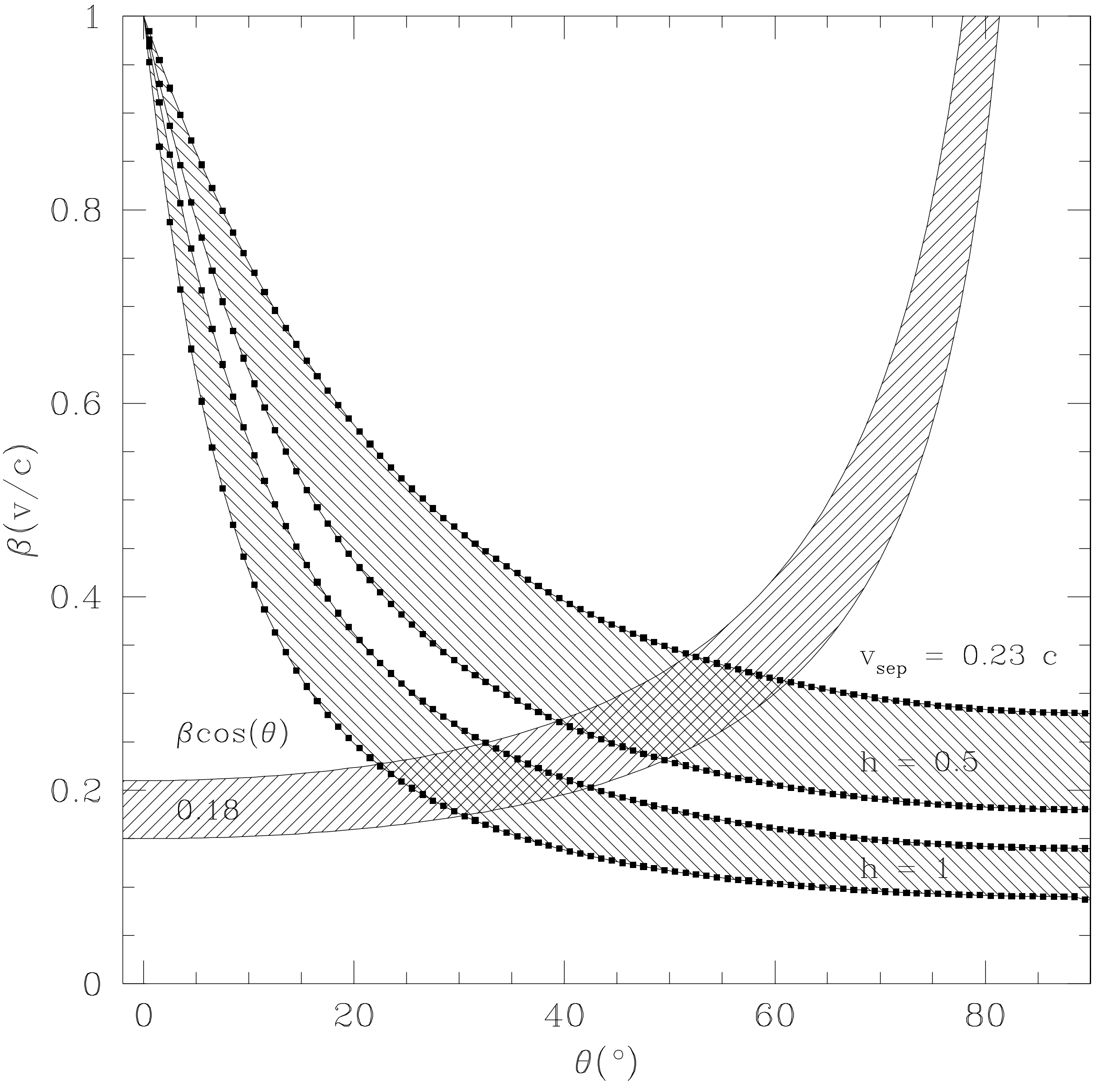

1
0.8
0.6
0.4
0.2
0
β(v/c)
0
20
40
60
80
θ(°)
v_{sep} = 0.23 c
βcos(θ)
0.18
h = 0.5
h = 1